One Earth

Article

Onset of runaway fragmentation of salt marshes

Graphical abstract

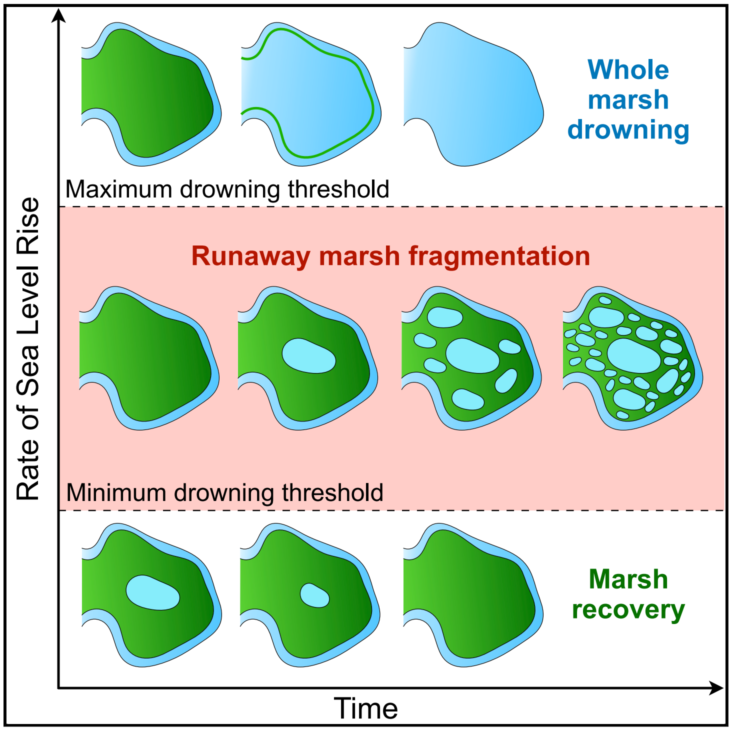

Highlights

- The sea level rise threshold for marsh drowning is lower than previously thought
- No marsh equilibrium after crossing the threshold for local marsh drowning
- Resilience of microtidal marshes depends weakly on inorganic sediment supply
- Predicted widespread loss of microtidal marshes through runaway fragmentation

Authors

Orencio Duran Vinent, Ellen R. Herbert, Daniel J. Coleman, Joshua D. Himmelstein, Matthew L. Kirwan

Correspondence

oduranvinent@tamu.edu

In brief

Salt marshes are among the most valuable and vulnerable ecosystems in the world. They adapt to sea level rise by accumulating organic and inorganic matter, but can locally drown above a certain sea level rise threshold. Using a process-based model, Duran Vinent et al. show that, beyond this threshold, the onset of local drowning leads to irreversible runaway fragmentation and widespread marsh loss, and that the extreme vulnerability of microtidal marshes arises from negligible inorganic sediment deposition in its interior.

Duran Vinent et al., 2021, One Earth *4*, 506–516
April 23, 2021
https://doi.org/10.1016/j.oneear.2021.02.013

CellPress

CellPress

Gold Standard for the Global Goals
3 tons of CO_2 offset

One Earth

Article

Onset of runaway fragmentation of salt marshes

Orencio Duran Vinent,[1,2,4,*] Ellen R. Herbert,[1,3] Daniel J. Coleman,[1] Joshua D. Himmelstein,[1] and Matthew L. Kirwan[1]
[1]Virginia Institute of Marine Sciences, College of William and Mary, Gloucester Point, VA 23062, USA
[2]Texas A&M University, Department of Ocean Engineering, College Station, TX 77843, USA
[3]Ducks Unlimited, Memphis, TN 38129, USA
[4]Lead contact
*Correspondence: oduranvinent@tamu.edu
https://doi.org/10.1016/j.oneear.2021.02.013

SCIENCE FOR SOCIETY We use a simplified formulation for sediment transport across marshes to explain why marshes are most vulnerable to sea level rise in microtidal environments (>60% of salt marshes in the US). We find that the fraction of a marsh that receives sediment scales positively with tidal range, so that only small portions of microtidal marshes receive significant sediment. Although marsh vulnerability has traditionally been thought to depend on flooding frequency and the suspended sediment concentration in local channels, we show that microtidal marshes must instead rely on the accumulation of plant roots to build soil. This organic accumulation has maximum rates comparable or lower than current rates of relative sea level rise rates measured at many microtidal marsh landscapes. Thus, we are currently at the tipping point for widespread drowning of global microtidal salt marshes regardless of the local inorganic sediment supply.

SUMMARY

Salt marshes are valuable but vulnerable coastal ecosystems that adapt to relative sea level rise (RSLR) by accumulating organic matter and inorganic sediment. The natural limit of these processes defines a threshold rate of RSLR beyond which marshes drown, resulting in ponding and conversion to open waters. We develop a simplified formulation for sediment transport across marshes to show that pond formation leads to runaway marsh fragmentation, a process characterized by a self-similar hierarchy of pond sizes with power-law distributions. We find the threshold for marsh fragmentation scales primarily with tidal range and that sediment supply is only relevant where tides are sufficient to transport sediment to the marsh interior. Thus the RSLR threshold is controlled by organic accretion in microtidal marshes regardless of the suspended sediment concentration at the marsh edge. This explains the observed fragmentation of microtidal marshes and suggests a tipping point for widespread marsh loss.

INTRODUCTION

There is a growing consensus that marsh vulnerability to relative sea level rise (RSLR) is tied to inorganic sediment availability,[1–4] where deposition of inorganic sediment increases with flooding duration, and potentially offsets sea level rise. Indeed, inorganic deposition rates have accelerated over the last century concomitant with sea level rise,[5,6] and historic marsh loss has been observed (and projected[7,8]) mostly in sediment-poor systems[9,10] and microtidal marshes.[11] Modeled threshold rates of RSLR for marsh drowning, using simplified point (0D) models, increase by 2 orders of magnitude as a function of suspended sediment concentration (SSC) and tidal range.[12,13] However, a contrasting body of work emphasizes the importance of organic matter accumulation in building marsh soils in the face of sea level rise, especially in the sediment-deficient estuaries most vulnerable to sea level rise.[1,11,14–17] Total marsh accretion rates are more strongly correlated with the organic fraction of marsh soil than the inorganic fraction[14]; organic matter contributes four times more soil volume than an equivalent mass of inorganic sediment[16]; and organic matter is the dominant contribution to marsh accretion by volume in many Atlantic and Gulf Coast marshes.[14–16]

Competing ideas about the relative importance of organic and inorganic accretion likely reflect strong spatial gradients within marshes.[18–20] Inorganic accretion increases with SSC and flooding depth, and decreases with distance to tidal channels, as reported both in the field[21–25] and in models.[18–20,26–29] Organic accretion is influenced by the production and decomposition of plant biomass, both of which vary spatially across marshes in

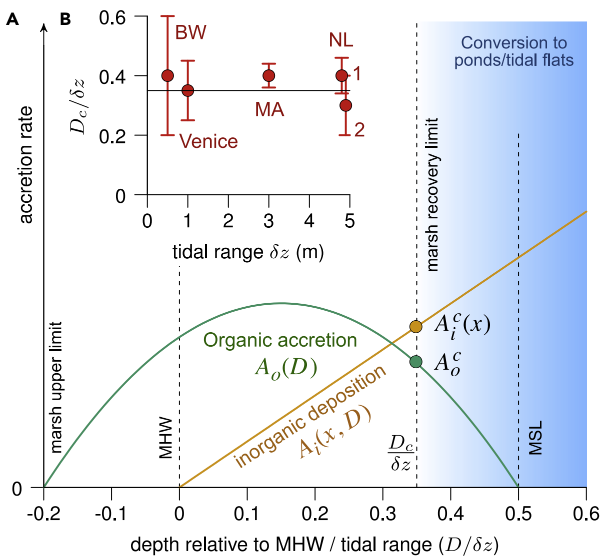

Figure 1. Critical depth for marsh recovery

(A) Sketch of the organic (A_o) and inorganic (A_i) accretion rates on a marsh platform as function of the local water depth (D) relative to mean high water level (MHW) and rescaled by tidal range δz. Accretion rates (A_i^c and A_o^c) at the critical depth for marsh recovery (D_c) determine the marsh response to sea level rise, where $A_i^c(x)$ is in general function of the distance x to sediment sources.

(B) Estimated values for the rescaled critical depth ($D_c/\delta z$) at different locations suggested by field data: Blackwater, MD (BW)[49]; Plum Island, MA (MA)[42]; Venice, Italy (general[47,48] and for San Felice marshes[49]); Hallegat and Paulina marshes, NL (NL 1)[43]; and Western Scheldt estuary, NL (NL 2)[46] (see Table S1 for details on the estimation of the critical depth and the site-specific definition of error bars).

response to flooding depth as well as other factors. Moreover, vegetation itself enhances inorganic sediment deposition so that organic and inorganic contributions are thoroughly intertwined.[30,31] These spatial gradients of organic and inorganic deposition lead to complex patterns of marsh accretion and submergence that are sometimes difficult to explain. For example, marshes along the Blackwater River (MD, USA) are rapidly submerging despite having higher SSCs measured in channels, than in nearby stable marshland.[32,33] Elsewhere, marshes are submerging despite measured accretion rates that are similar to or exceed RSLR,[2,33] which suggests that measurements take place mostly along marsh edges, where maximum accretion rates are generally observed.[21,23,34,35]

The complexity of organic and inorganic accretion in a marsh platform leads to the simple question: Where in a marsh should organic and inorganic contributions to marsh accretion be characterized to best evaluate marsh vulnerability to RSLR? Measurements from high elevation portions of a marsh potentially underestimate future marsh accretion because inorganic accretion rates may accelerate with increased flooding duration.[2] However, if low elevation marshes are also closest to channels, then accretion rates from low elevation portions of the marsh would overestimate accretion to the marsh as a whole, and lead to an underestimation of marsh vulnerability to RSLR.

Another issue with the interpretation of measured accretion rates is that they tend to converge toward the local rate of RSLR, as the marsh platform approaches an equilibrium elevation,[36] which complicates the estimation of maximum accretion rates unless marshes are already drowning.[2,37] Thus, there is a need for better numerical models that resolve the spatial complexity of marsh sediment dynamics.[4,13,19,27,28,38–40]

A few existing process-based models (e.g., Ratliff et al.[19] and Da Lio et al.[28]) capture the observed drowning of interior marshes and their conversion to ponds.[41–43] They suggest marsh drowning, and subsequent pond formation, is not described by a single threshold but is instead a gradual process where different portions of the marsh platform drown at different rates of RSLR. Therefore, existing models with RSLR rates just slightly faster than the threshold for drowning would produce an equilibrium state characterized by relatively few, isolated ponds, far from the channel edge.

Here, we uniquely show that there is no equilibrium state for a marsh platform once a local threshold for marsh drowning has been crossed, resulting in runaway marsh fragmentation. Theoretical considerations and field observations indicate that the threshold for marsh drowning does not change much with sediment supply in microtidal marshes, suggesting a disproportionate role of organic accretion.

Model approach

We use a one-dimensional formulation for the mass conservation of water and inorganic sediments, in the absence of erosion,[4,27,28,38,39,44] to derive a minimal sediment transport model that captures the central physics of the system (the complete model is described in the experimental procedures; see Figures S1 and S2 for examples of the solutions). This simplified model allows us to define and calculate the drowning threshold and characterize the dynamics of the ensuing marsh fragmentation without the need of spatially explicit hydrodynamic models.[26,27,29,39,45]

The current understanding of the onset of marsh loss is that it takes place whenever marsh depth relative to mean high water is higher than a critical value D_c above which marshes are replaced by tidal flats or ponds as the more stable morphology.[43,46–49] Indeed, field data suggest that marsh conversion to tidal flats starts at a critical depth D_c around 35% of the tidal range δz, which corresponds to an average rescaled inundation time, i.e., fraction of time the marsh is submerged $\tau_c \approx \pi^{-1}\arccos(1 - 2D_c/\delta z)$, of about 0.4 (Figure 1B, see Table S1 for details).[42,43,46–48]

Assuming the existence of a critical depth for marsh recovery, a general condition for the onset of local marsh drowning is when the rate R of RSLR exceeds the sum of the organic (A_o^c) and inorganic (A_i^c) accretion rates evaluated at the critical depth D_c (Figure 1A). Because of the spatial variation of inorganic deposition, the lowest inorganic accretion rate at the critical depth thus defines the lowest threshold (R_c) for local marsh drowning: $R_c = A_o^c + \min\{A_i^c\}$.

We derive a general expression for R_c from a simplified model of the inorganic accretion rate $A_i(x, D)$ across a marsh platform with variable depth $D(x)$, as function of the distance x to the sediment sources. In the absence of erosion, we assume $A_i(x, D)$ can be written in terms of the depth-dependent rescaled average inundation time $\tau(D)$ and the depth-independent sediment concentration $\overline{C}(x)$, as $A_i(x, D) = \rho_i^{-1} w_f \tau(D)\, \overline{C}(x)$, where ρ_i is an

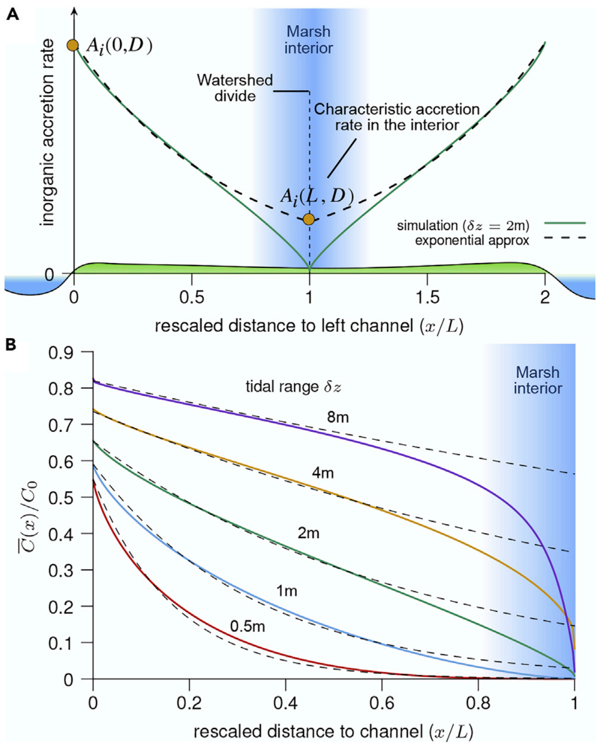

Figure 2. Spatial decay of sediment concentration and scaling with tidal range

Simulation and exponential approximation of the decay of the average sediment concentration $\overline{C}$ with the rescaled distance from channel x/L, where L is the length of the drainage basin. For illustration purposes we show in (A) the inorganic accretion rate for a constant marsh depth D—such that $A_i(x,D) \propto \overline{C}(x)$—where $A_i(0,D)$ is the accretion rate at the marsh edge and $A_i(L,D)$ is the characteristic accretion rate in the marsh interior. (B) Rescaled $\overline{C}/C_0$ simulated for simplicity for constant marsh depth and varying tidal range δz (solid lines). The effective sediment falling velocity is $w_f = 10^{-4}$ m/s and the tidal period is T = 12.5h. Dashed lines show the exponential approximation $\overline{C}(x) = \overline{C}(0)e^{-x/L_c}$ with L_c given by Equation 2.

average density of deposited sediments,[1] w_f is an effective settling velocity, and $\overline{C}$ is defined as the local depth-averaged SSC averaged over times of positive water depths in a tidal cycle (see experimental procedures).

In what follows we present and validate an explicit expression for the inorganic accretion rate across the marsh platform and use it to obtain the critical inorganic accretion rate for marsh drowning. We then introduce the drowning threshold, characterize the runaway marsh fragmentation regime, and discuss the effect of external parameters on marsh drowning.

RESULTS

Exponential decay of sediment concentration

As inorganic sediments in the water column settle on the marsh surface, where erosion is assumed to be negligible,[27] the averaged sediment concentration $\overline{C}$ decays with the distance x from the channel or tidal flat (Figure 2). Sediment concentration thus reaches its lowest value at the location furthest away—a distance L—from marsh edges (Figure 2A), defined in the model as the watershed divide. This decay in sediment concentration is well approximated by an exponential function, $\overline{C}(x) = \overline{C}(0)e^{-x/L_c}$ (as proposed by Fagherazzi et al.[25] and observed by Temmerman et al.[23]), with decay length L_c (see experimental procedures). Therefore, the inorganic accretion rate for a non-flat marsh platform can be approximated as

$$A_i(x, D(x)) \approx \rho_i^{-1} w_f \tau(D(x)) \overline{C}(0) e^{-x/L_c}, \qquad \text{(Equation 1)}$$

where the average sediment concentration $\overline{C}(0)$ at the channel bank or marsh edge is proportional to the average concentration C_0 at the channel or mud flat during flood (see Figure S3 for the proportionality factor).

The decay length L_c of the average SSC scales as the ratio of the tidal discharge per unit width and the effective sediment settling velocity w_f, in agreement with the scaling of the deposition length in unidirectional turbulent suspensions[50] (experimental procedures). We find tidal discharge per unit width scales as $L\delta z/T$, where δz is the tidal range, T is the tidal period and, L is the characteristic length of the local drainage basin. Thus, the decay length has the form

$$L_c = \beta L \delta z/(T w_f), \qquad \text{(Equation 2)}$$

with fitting parameter $\beta \approx 1.5$, in agreement with both numerical simulations and analytical approximations (experimental procedures and Figure 2B).

We find the exponential approximation accurately describes the sediment concentration profile except in the region around the watershed divide, where tidal flow stops and the simulated average sediment concentration, and thus accretion rates, converge to zero (Figure 2). In reality, complex tidal flows may lead to residual accretion rates in the marsh interior (e.g., Christiansen et al.[22]), in which case the exponential approximation provides an upper limit to evaluate the resiliency of drowning marshes. In what follows we use the watershed divide as a formal definition of the marsh interior.

The exponential decay correctly predicts the spatial gradient in the average sediment concentration and inorganic accretion rates for a wide variety of salt marshes (Figure 3), including low elevation microtidal marshes in the Virginia Eastern Shore (Phillips Creek)[34] and Georgia[35], and meso- and macrotidal marshes in Plum Island, MA[51], Norfolk, UK,[21] and in the Bay of Fundy, CA[52] (see experimental procedures for further details on the analysis and interpretation of inorganic accretion data).

The scaling of L_c with the tidal range δz (Equation 2) means that suspended sediments deposit closer to channels (or tidal flats) at lower tidal ranges, whereas they are more homogeneously distributed at higher tidal ranges. This is consistent with the trend observed in field measurements (Figure 3), in particular the contrast between the almost homogeneous inorganic accretion in the Bay of Fundy, CA[52] (δz = 11m), and the noticeable decay observed in Phillips Creek, USA[25] (δz = 2m).

Critical inorganic accretion rate

The scaling of the sediment decay length L_c with the local drainage basin length L (Equation 2) follows from the approximate scale invariance of tidal flows,[44] i.e., faster flows—and

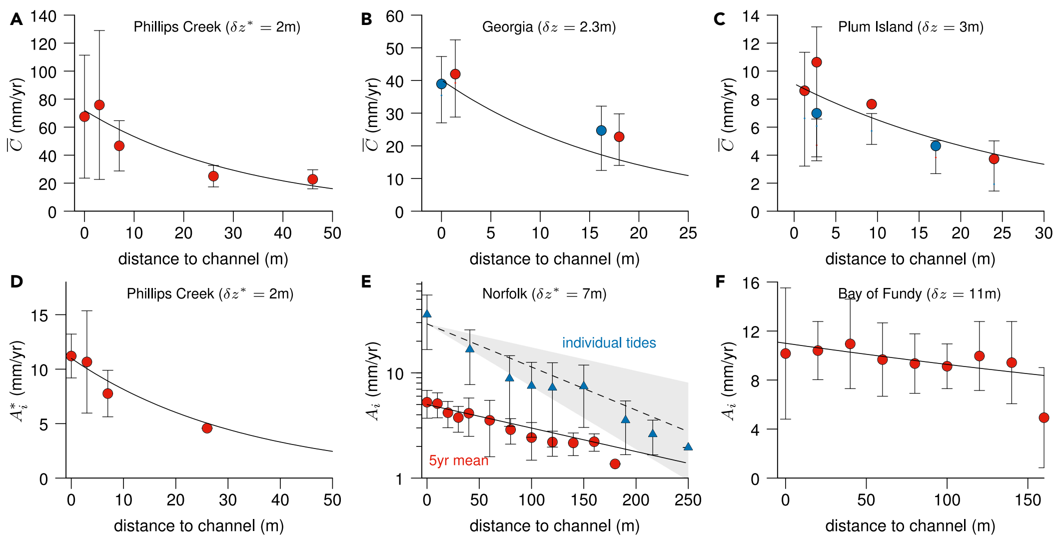

Figure 3. Validation of the exponential decay of sediment concentration and inorganic accretion

Proposed exponential decay (lines) compared to measurements of averaged sediment concentration $\overline{C}$ (A,[34] B,[35] and C[51]) and inorganic accretion rate A_i (D,[34] E,[21] and F[52]) (symbols). A_i^* is the depth-corrected accretion rate (see experimental procedures for more information). The scaling of the decay length is obtained from the model as $L_c = 1.5L\delta z/(Tw_f)$ (e.g., Equation 2), where δz is the tidal range, T is tidal period, and w_f is the effective sediment falling velocity. In all cases L is taken as the maximum distance to a channel reported in the data, δz (δz^*) is the reported tidal range (average/typical tidal range during the measurement period), and we use the generic value $w_f = 10^{-4}$m/s[3,22,53] unless stated otherwise. Values of $\overline{C}(0)$ and $A_i(0)$ were fitted to data. Mass accretion rate data were converted to volume accretion rate using an effective density of inorganic sediments deposited in the marsh $\rho_i \approx 2$g/cm^3.[1] All symbols correspond to the average of reported values. Error bars in (A, D, and F) represent the standard deviation of the measurements, whereas in (B) and (C) they represent the 25th and 75th percentiles. Error bars in (E) represent either the standard deviation (5-year mean data, circles) or the range (individual-tide data, triangles) of reported data. Colors in (B and C) correspond to different measurement periods. In (A), $\overline{C}$ is calculated as the mean of the reported maximum concentrations measured during flood and ebb. In (E), we assume $w_f = 3 \times 10^{-4}$m/s, which is the lowest value of the reported range of settling velocities ($w_f = 3 - 8 \times 10^{-4}$m/s) to fit the long-term measurements (solid line), whereas we use the average value, $w_f = (5.5 \pm 2.5) \times 10^{-4}$m/s, for measurements during single tides (dashed line and shaded area). In both cases the effective tidal range $\delta z^* = 7$m is the average of the reported range $6 - 8$m.[21]

increasing sediment advection—on larger basins. This scale invariance, where sediments are deposited farther away from the channels in large basins as compared to small ones (Figure S4), has one important implication: the lowest inorganic accretion rate at the critical depth D_c for marsh conversion to tidal flats $A_i^c(L) \equiv A_i(L, D_c)$, reached at the watershed divide $x = L$ (Equation 1), does not depend on drainage basin size L and can be evaluated without the need of spatially explicit hydrodynamic models. Indeed, after substituting the scaling for the decay length we get for the critical inorganic accretion rate:

$$A_i^c(L) = A_i^c(0)e^{-1/\ell_c}\ , \qquad \text{(Equation 3)}$$

where $\ell_c = L_c/L = \beta/w_f^+$ is the rescaled decay length, which only depends on the rescaled effective falling velocity $w_f^+ = w_f T/\delta z$, and $A_i^c(0) \equiv A_i(0, D_c)$ is the inorganic accretion rate at the critical depth in the marsh edge (Equation 1). Using the scaling $\overline{C}(0) = r(w_f^+)C_0$, we find for the flood-ebb average sediment concentration at the marsh edge (see experimental procedures), we get the explicit expression

$$A_i^c(0) = \rho_i^{-1} C_0 w_f r(w_f^+)\tau_c\ , \qquad \text{(Equation 4)}$$

with $\tau_c \equiv \tau(D_c)$. Thus, the critical inorganic accretion rate (Equation 3) is completely determined by external, measurable parameters, characterizing sediment supply to the marsh (C_0), effective sediment properties (w_f and ρ_i), and tides (δz and T).

An important consequence of the physical mechanisms driving sediment redistribution across the marsh platform, as summarized in Equation 3, is that the critical inorganic accretion rate strongly depends on the tidal range (Figure 4). For typical values of the parameters, $A_i^c(L)$ becomes negligible for tidal ranges δz<1 m regardless of the sediment supply (Figure 4), in stark contrast to the critical inorganic accretion rate at the marsh edge $A_i^c(0)$ (Figure 4A). More generally, for most microtidal marshes (δz<1.5m) the predicted critical accretion rate in the marsh interior ($A_i^c(L)$) is below common rates of RSLR (2.5–5 mm/year) (Figure 4B) and organic accretion becomes crucial for marsh survival.

Threshold for marsh drowning and the onset of runaway marsh fragmentation

The marsh accretion rate at the critical depth in the marsh interior, $A_o^c + A_i^c(L)$, defines the lowest threshold for marsh drowning R_c (Figure 5A). When relative sea level rises at a lower rate (R<R_c), marshes are stable by definition and bare areas with an elevation above the critical depth can recover with time.[42] When relative sea level rises at a faster rate (R>R_c), interior marshes drown and form permanent ponds.

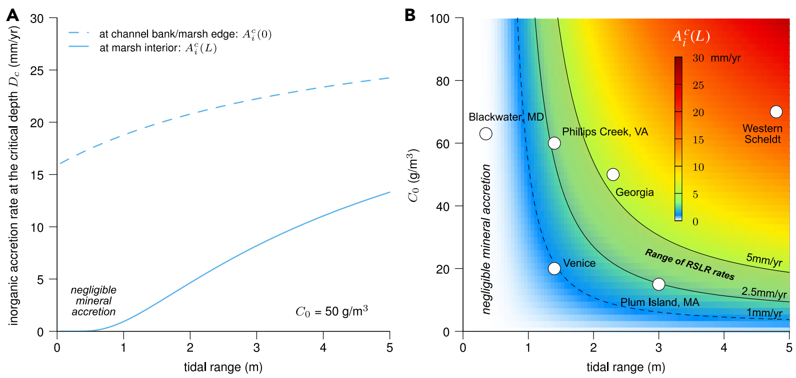

Figure 4. Predictions of critical inorganic accretion rates

(A) Inorganic accretion rates at the critical depth D_c evaluated at the marsh edge and marsh interior ($A_i^c(0)$ and $A_i^c(L)$, respectively) as function of tidal ranges for an average suspended sediment concentration at the channel bank of $C_0 = 50 g/m^3$. We use $w_f = 10^{-4}$ m/s, which is within commonly reported ranges[3,22,53] and $\rho_i = 2 g/cm^3$, obtained from a meta-analysis of bulk density measurements in global marshes.[1]

(B) Color map of the critical inorganic accretion rate at the marsh interior $A_i^c(L)$ as function of tidal range and average SSC at the channel bank (C_0). Black lines separate regions with low inorganic deposition in the marsh interior ($0A_i^c(L)<1$ mm/year, dashed line) and with inorganic deposition lower than a common range of global rates of RSLR ($A_i^c(L)<2.5 - 5$ mm/year, solid lines). Superimposed data: Venice, Italy[3]; Western Scheldt, NL[53]; from USA: Blackwater, MD[33]; Plum Island, MA[42,51]; Phillips Creek, VA[22,34]; Georgia.[35]

Simulations of the time evolution of marsh elevation $Z(x,t)$ (see experimental procedures for model details), show marsh fragmentation regime strongly depends on whether permanent ponds are isolated or connected to the channel network (Figure 5A). In the first case, tidal basins and watershed divides remain unchanged and the system evolves toward a new equilibrium state (Figure 5A, left). The portion of the marsh closer to the edge adapts to RSLR and reaches a non-uniform equilibrium marsh elevation in response to spatial gradients of sediment concentration, e.g., as in the formation of natural levees.[56] We find the equilibrium pond size scales with the size of the local basin and increases with the rate R of RSLR (Figure 5A, left, see experimental procedures for pond size calculation).

However, isolated ponds tend to connect to the channel network via the formation of new small channels,[41,42,49] thereby increasing channel density and shrinking tidal basins. Based on this, we assume in our model that once ponds are deep enough they connect to channels and become a source of sediment and tidal flow (see experimental procedures). Regardless of the specific conditions for when and how ponds connect, simulations show there is no marsh equilibrium as long as permanent ponds are able to connect to the channel network. Instead, marshes experience a continuous (runaway) fragmentation at a rate controlled by the ratio R/R_c (Figure 5A, right).

The runaway fragmentation can be understood as follows: although there are more channels (and connected ponds) to potentially redistribute sediments into the marsh platform, the sediment will be deposited closer to the banks as water flow slows down in the now smaller basins (see Equation 2). As a result, the drowning threshold $R_c = A_o^c + A_i^c(L)$ is crossed around the watershed divide of the new system, leading to marsh drowning at ever smaller scales. Therefore, with time, marsh fragmentation propagates from large to small scales following the adjustment of the channel network and tidal flows, until most of the marsh is lost.

We can obtain an upper-bound for the threshold rate of RSLR for the onset of runaway marsh fragmentation ($R_c = A_o^c + A_i^c(L)$; Figure 6) using a theoretical estimation of the maximum contribution of organic accretion for salt marshes[1] ($A_o^c \approx 3$mm/year). This value is consistent with accretion rate data of Mid-Atlantic US salt marshes and falls within a broader range of direct and indirect estimations of organic accretion rates of marshes elsewhere (see Figure S5 and supplemental experimental procedures). Similarly to the trend of inorganic accretion rates with tidal range (Figure 4), the predicted threshold R_c (Figure 6) shows a fundamental vulnerability for microtidal marshes ($\delta z<1.5$m) and marshes with relatively low sediment supply (average SSC at the channel bank or marsh edge in the range $C_0<20 g/m^3$).

Self-similarity of marsh fragmentation and power-law distribution of pond size

Because pond size scales with basin size (see experimental procedures), the progressive shrinking of tidal basins during marsh fragmentation should lead to a self-similar hierarchy of pond sizes with a Pareto (power-law) distribution.[57] Indeed, we find a power-law distribution of pond areas and a self-similar pattern of marsh loss, in both our model simulations of marsh fragmentation (shown in Figure 5A, where pond area is defined as the square of its length) and in rapidly submerging marshes in Blackwater, MD, and Louisiana (Figure 5), where drowning begins near the watershed divide and propagates toward the channels.[41]

Interestingly, the exponent of the power-law distribution of the area of simulated ponds changes little with the rate of RSLR above the threshold R_c, and is very similar to the one obtained for small to medium size ponds ($\lesssim 10^5 m^2$) in Blackwater[54] (Figure 5B). The exponent ($\sim$1.5) is consistent with a simple "period-doubling" mechanism, where whenever a pond connects to the channel network it creates two new ponds with half the diameter (one-quarter of the area) of the "parent" one.

The size distribution of large ponds in Louisiana[55] has a larger exponent ($\sim$2.5) similar to the one for similar-size ponds in Blackwater (Figure 5B), which suggests a further scale-invariant mechanism affecting pond growth.

DISCUSSION

Vulnerability of microtidal marshes

Although marsh vulnerability has been traditionally tied to inorganic sediment availability, we find consistently low inorganic accretion in the interior of most microtidal marshes ($\lesssim$ 2.5 mm mm/year, one-sixth of existing predictions, e.g., Dalpaos,[18] Ratliff et al.,[19] and Da Lio et al.[28]) (see Figure 4B)

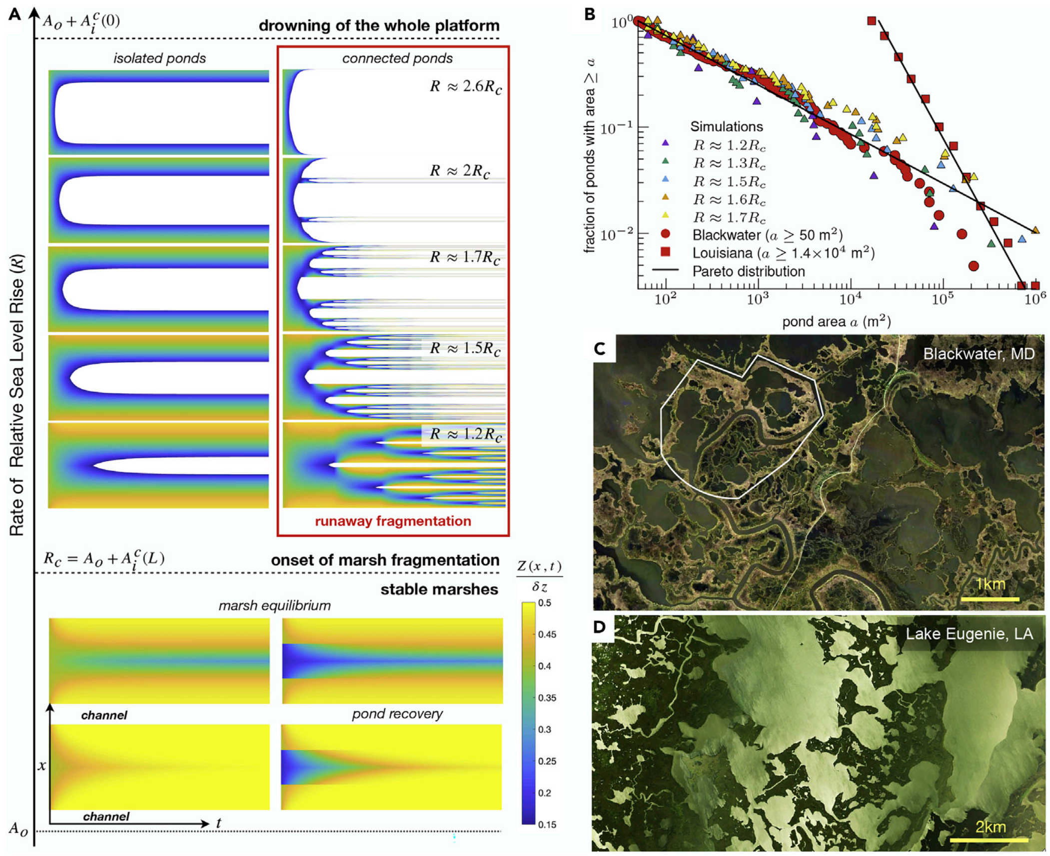

Figure 5. Marsh equilibrium states and runaway marsh fragmentation

(A) One-dimensional spatiotemporal plots of simulated marsh elevation $Z(x,t)$ (in color) for different rates R of RSLR starting from a flat marsh platform flanked by channels on both sides (see Methods for model description and parameters). For each rectangle, x runs vertically from channel to channel and t runs from left to right (see bottom left illustration). Elevations below the critical value $Z_c/\delta z = 0.15$ (corresponding to $D_c/\delta z = 0.35$) are shown in white and represent ponds. For $R < R_c$, shallow ponds can recover (bottom center) and marshes reach a non-flat equilibrium state. For $R > R_c$, the marsh drowns and forms ponds. If those ponds remain isolated, the marsh eventually reaches equilibrium. Otherwise, a self-similar mechanism of pond formation and basin reduction leads to a runaway marsh fragmentation.

(B) Exceedance probability distribution of pond areas in Blackwater, MD (representing ponds larger than 50 m^2 within the white region in (C) (see Himmelstein[54] for details on data acquisition; data available in Table S2) and Louisiana (reported ponds larger than 1.4×10^4 m^2 obtained from 1982 to 1985 composite satellite images[55]). The distribution of simulated ponds (A) (with pond area defined as the square of its length) is shown for comparison. The distribution of pond area is consistent with a Pareto (power-law) distribution (linear fits), with power 1.46 for Blackwater, 2.6 for Louisiana, and ~ 1.5 for the simulations.

(C and D) Examples of apparently self-similar patterns from marshes in Blackwater, MD, and around Lake Eugenie, LA.

regardless of sediment supply. This vulnerability is highest for marshes with tidal ranges <1 m (Figure 4B), where inorganic accretion in the marsh interior is negligible and the threshold RSLR rate seems to be completely determined by organic accretion. This explains the apparent contradiction of Blackwater marshes, where a relatively high SSC in the channels does not prevent drowning.[32,33] With a tidal range <0.5 m, inorganic accretion is irrelevant for the vast majority of the marsh platform. Thus, it is enough for the local rate of RSLR to be higher than the organic accretion rate to induce widespread drowning (Figure 6). This indeed seems to be the case in both Blackwater[58] and in the Mississippi Delta, where the threshold for continuous marsh loss was estimated to be about 3 mm/year[59], very similar to model prediction for δz<1 m (Figure 6). The predicted low inorganic deposition in the marsh interior also agrees with the predominantly organic composition of sediments found in many marshes with tidal range <1 m (e.g., Blackwater, MD[58]; Gulf of Mexico[14]).

While organic accretion is a complex function of several factors, such as plant species, water salinity, flooding frequency, and water and soil temperature and composition,[10,16] a meta-analysis of field data reveals that organic accretion rates are in the range of 3.0 ± 2.0 mm/year (Figure S5 and supplemental experimental procedures), which happens to be in the range of observed RSLR rates. Therefore, it seems we currently are at the tipping point for widespread drowning of global microtidal salt marshes regardless of the local inorganic sediment supply (Figure 6). Indeed, the model correctly predicts the drowning of Blackwater marshes and marshes in the Mississippi Delta,[59] and also suggests marshes in Venice, the Virginia Eastern Shore

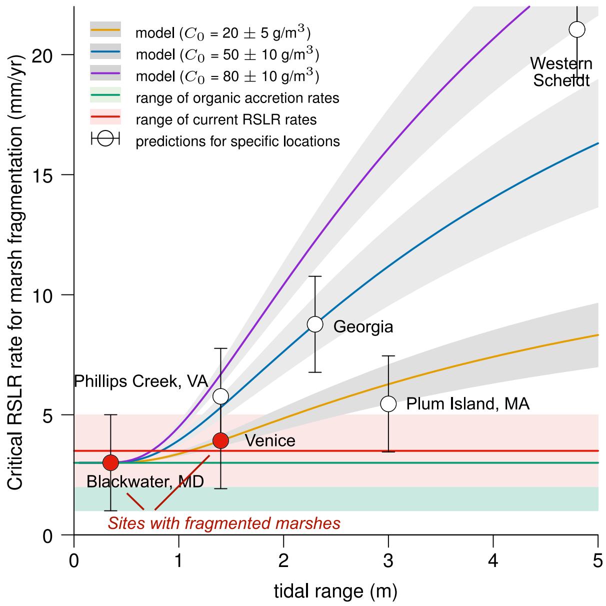

Figure 6. Threshold rates for runaway marsh fragmentation

Lines are predicted thresholds for marsh fragmentation ($R_c = A_o^c + A_i^c(L)$) as function of tidal range, for different values of the average suspended sediment concentration at the channel bank C_0 representing typical low, mid, and high sediment supply conditions (see Figure 4B). We use $w_f = 10^{-4}$ m/s and ρ_i = 2 g/cm^3 for the calculation of the critical inorganic accretion $A_i^c(L)$ (as in Figure 4), and assume an organic accretion rate A_o^c = 3mm/year, consistent with a meta-analysis of field data (Figure S5 and supplemental experimental procedures). Symbols represent predictions for specific locations, including Blackwater, MD; Plum Island, MA; Phillips Creek, VA, and Georgia (we use values shown in Figure 4B). Error bars denote the uncertainty in the estimated organic accretion rate, of the order of 2 mm/year (see Figure S5 and supplemental experimental procedures). Current RSLR rates for those locations are in the range 3.5 ± 1.5mm/year (red line and shaded area). Organic accretion rates in salt marshes are in the range 3.0 ± 2.0mm/year (green line and shaded area, see Figure S5 and supplemental experimental procedures).

(e.g., Phillips Creek), and Plum Island, MA, are particularly vulnerable (Figure 6).

We thus provide a mechanistic explanation for the widely observed fragility of microtidal marshes[11] and show this vulnerability is intrinsic and tied to the dominant role of organic accretion. Therefore, factors altering biomass productivity and decomposition, such as eutrophication, increased CO_2, and climate warming,[10,11,19,60] could decide the mid-term response of global microtidal marshes, while measures aimed at increasing sediment delivery could have limited success.

Runaway marsh fragmentation

The runaway marsh fragmentation induced by the approximate scale invariance of sediment deposition,[44] constitutes a new form of marsh destabilization that transforms the local crossing of the marsh drowning threshold into the onset of eventual widespread marsh loss. This mechanism only requires that connected ponds decrease the size of local drainage basins, regardless of whether they deliver sediment to the marsh platform or not. In the best case scenario depicted in Figure 5A, connected ponds redistribute inorganic sediment as effective as large channels or mud flats, which is not the case in reality. Any decrease in sediment delivered by connected ponds leads to lower inorganic accretion rates on the surrounding marshes, thereby accelerating marsh drowning.

The scale invariance of sediment deposition, where sediment is deposited closer to the banks in smaller basins, underpinning the runaway marsh fragmentation is consistent with observations that an increased density of artificial channels does not increase overall sedimentation (e.g., Louisiana[61]) and in some cases resulted in subsidence (e.g., New England[62]). Furthermore, the predicted acceleration of marsh fragmentation with the rate of RSLR (Figure 5A) is consistent with the rapidly increased rate of historic marsh loss measured in the Mississippi Delta as RSLR accelerated.[59]

The marsh fragmentation mechanism explains the formation of a broad range of pond sizes, and predicts that their size distribution should follow a power-law, in agreement with data from Blackwater marshes (Figure 5B). It also predicts a particular temporal sequence of marsh fragmentation, as large initial ponds eventually lead to smaller ones at a rate increasing with the rate of RSLR relative to the drowning threshold (Figure 5A), and suggests that the area of the larger ponds depends on the initial distribution of tidal basin areas. This multi-scale mechanism complements existing models of pond growth driven by lateral expansion instead of RSLR.[40,63]

Conclusions

We derive a simplified model of sediment transport in the absence of erosion that explains patterns of sediment deposition and marsh vulnerability in a wide variety of conditions. Our model leads to an analytical prediction of inorganic accretion that complements direct measurements of accretion, which necessarily reflect historical rather than future environmental conditions.[2] We predict a new form of marsh destabilization characterized by a progressive fragmentation of the marsh platform, triggered by the drowning of interior marshes. The threshold for this runaway marsh fragmentation is much lower than existing predictions[13,64] and is largely decoupled from inorganic sediment supply in microtidal environments, which explains the observed fragility of microtidal marshes. Beyond microtidal marshes, the much lower marsh fragmentation thresholds predicted by our model suggest a re-evaluation of the resiliency of global marshes under current and future scenarios.[64]

EXPERIMENTAL PROCEDURES

Resource availability

Lead contact

Further information and requests for resources and reagents should be directed to and will be fulfilled by the lead contact, Orencio Duran Vinent (oduranvinent@tamu.edu).

Materials availability

The original (unpublished) data used in this study is available in Table S2.

Data and code availability

This study did not generate new datasets. The MATLAB code integrating the model equations is available upon request from the lead contact.

Minimal model of sediment transport on a marsh

We consider one-dimensional depth-integrated mass conservation equations for tidal water discharge per unit width $Q(x,t)$ and depth-averaged SSC of inorganic sediments $C(x,t)$ over a marsh surface with elevation $Z(x)$ relative to mean sea level (MSL). Assuming, (1) a quasi-static tidal propagation with average water elevation (relative to MSL) $\eta(t)=(\delta z/2)\cos(2\pi t/T)$ with tidal range δz and period T, (2) no net sediment erosion, and (3) negligible lateral diffusion, the conservation of suspended sediments reads[4,27,28,38,39,44]:

$$\partial_t(HC) + \partial_x(QC) = -w_f C, \qquad \text{(Equation 5)}$$

where x is the distance from the marsh edge (channel bank or tidal flat) along the flow direction, $H(x,t)=\eta(t)-Z(x)$ is local water depth, and w_f is an effective sediment falling velocity. Q is obtained from the continuity equation $\partial_x Q = -\partial_t \eta$ assuming no water flux ($Q(L,t)=0$) at the watershed divide $x=L$: $Q(x,t) = \partial_t\eta\,(L-x) = -\delta z L T^{-1}\pi\sin(2\pi t/T)\,(1-x/L)$. Q thus scales as $\delta zL/T$.

For simplicity, Equation 5 is numerically integrated for a flat marsh surface during positive water depths ($H(t)>0$) using two boundary conditions, a constant SSC ($C(0,t)=C_0$) at the channel bank ($x=0$) during flood ($t<0$) and no sediment crossing the watershed divide ($C(L,t)=0$) during ebb ($t>0$). Using rescaled time ($t^+=t/T$) and distance ($x^+=x/L$), the rescaled concentration $C(x^+,t^+)/C_0$ for a given marsh elevation Z is only a function of one dimensionless number: the rescaled effective falling velocity $w_f^+=w_fT/\delta z$ (Figure S1).

Approximation for the tidal-averaged sediment transport

A further simplification is obtained by averaging Equation 5, valid for a non-flat marsh elevation $Z(x)$, over times of positive water depths in a tidal cycle, and neglecting the changes to the gradient of sediment fluxes (QC) due to variable elevation,

$$\partial_x\overline{QC} \approx -w_f\overline{C}, \qquad \text{(Equation 6)}$$

where the bar denotes an average of the form

$$\overline{C}(x)\equiv\tau(D)^{-1}\int_{-\tau(D)/2}^{\tau(D)/2} C(x,t^+)\,dt^+, \qquad \text{(Equation 7)}$$

where $\tau(D)$ is the rescaled local inundation time and $D(x)=\delta z/2-Z(x)$ is the local depth.

Because the main effect of a non-flat marsh platform is to change the local inundation time $\tau(D)$, this averaging removes, in a first approximation, the dependence on marsh elevation and thus its solution has the form $\overline{C}\approx\overline{C}(x)$. Therefore, we can use the numerical solution of Equation 5 for a flat marsh to obtain a correlation between the average sediment flux per unit width ($\overline{QC}$) and the average SSC ($\overline{C}$). This correlation is expected when transport is dominated by advection instead of diffusion.

Indeed, in the range $x/L\lesssim 0.6$, we find (see Figure S2)

$$\overline{QC}(x)\approx\beta\delta zLT^{-1}\left(\overline{C}(x)-\overline{C}(L)\right), \qquad \text{(Equation 8)}$$

where $\beta=1.5$ is a fitting constant and $\overline{C}(L)$ is defined as an effective sediment concentration at the watershed divide $x=L$. This definition follows from the boundary condition of no average sediment transport across the watershed divide, i.e., $\overline{QC}(L)=0$. Using Equation 8, the total mass of sediment deposited on the one-dimensional marsh during one tidal cycle, $\tau(D)T\int_0^L w_f\overline{C}(x)dx$, can be approximated by integrating Equation 6 as $\overline{QC}(0)\tau(D)T\approx\beta\delta zL\tau(D)(\overline{C}(0)-\overline{C}(L))$.

Substituting the advection approximation (Equation 8) into Equation 6, we get an equation for the average SSC

$$\beta L\partial_x\overline{C}\approx -w_f^+\overline{C}, \qquad \text{(Equation 9)}$$

which has the exponentially decaying solution

$$\overline{C}(x) = \overline{C}(0)\exp(-x/L_c), \qquad \text{(Equation 10)}$$

with decay length $L_c=\beta L/w_f^+$ or $L_c=\beta L\delta z/(Tw_f)$ after substituting w_f^+.

From Equation 6, the scaling of the decay length has the more general form $L_c\propto Q/w_f$ (as can be verified using $Q\propto\delta zL/T$), which is equivalent to the scaling of the decay or deposition length in unidirectional turbulent suspensions[50]: $L_c\propto HU/w_f\propto Q/w_f\partial$, where H is the flow depth, U is the (constant) flow velocity, and $Q\propto UH$ is the water discharge per unit width.

Finally, the boundary condition $\overline{C}(0)$ in Equation 10 is obtained numerically from Equation 5 by averaging $C(0,t)$ over one tidal cycle, which gives (see Figure S3)

$$\overline{C}(0) = C_0 r(w_f^+), \qquad \text{(Equation 11)}$$

with fitting function

$$r(w_f^+) = \left(1+\left(1+w_f^+\right)^{-1}\right)/2. \qquad \text{(Equation 12)}$$

This function quantifies the average sediment concentration of the ebb flow leaving the marsh platform. Defining $\overline{C}(0)\equiv[\overline{C}_{\text{flood}}(0)+\overline{C}_{\text{ebb}}(0)]/2$, substituting Equations 11 and 12, and using our assumption of a constant concentration at the marsh edge during flood ($\overline{C}_{\text{flood}}(0)=C_0$), we get,

$$\overline{C}_{\text{ebb}}(0) = C_0\left(2r(w_f^+)-1\right)=C_0/\left(1+w_f^+\right). \qquad \text{(Equation 13)}$$

For small tidal ranges, the rescaled falling velocity diverges, $\overline{C}_{\text{ebb}}(0)\rightarrow 0$ and most of the sediment is deposited on the marsh. For large tidal ranges, the opposite is true, $w_f^+\rightarrow 0$ and $\overline{C}_{\text{ebb}}(0)\rightarrow C_0$, i.e., most of the sediment leaves the marsh.

Inorganic accretion rate

In the absence of erosion, the net inorganic accretion rate averaged over a tidal cycle is defined as the volume of inorganic sediments suspended in the water column that settles on the marsh surface per unit area and unit time, and can be approximated as $A_i(x,D) = \rho_i^{-1}w_f\tau(D)\overline{C}(x)$, where ρ_i is the long-term averaged density of deposited sediments[1] and $\tau(D)\approx\pi^{-1}\arccos(1-2D/\delta z)$ is the average rescaled inundation time. Using Equation 10, $A_i(x,D)$ can be approximated as

$$A_i(x,D)\approx\rho_i^{-1}C_0 r(w_f^+)w_f\tau(D)\exp(-x/L_c). \qquad \text{(Equation 14)}$$

In general, sediment transport properties (C_0, L_c, D, $\tau(D)$, etc.) change with tidal range. However, in what follows (as within the main text) we assume the average inorganic accretion rate can be simply calculated by Equation 14 evaluated at a mean tidal range, denoted as δz for simplicity. When comparing with field data, δz is the mean over the measurement period, otherwise we use a representative value.

Simplified one-dimensional model of marsh dynamics

To calculate the response of the marsh/mud elevation, $Z(x,t) = \delta z/2 - D(x,t)$, to a rate R of RSLR, we propose a minimal model for the total accretion rate $\partial_t Z$ as a function of the local elevation that describes: (1) marsh drowning, (2) the formation of isolated ponds, and (3) the changes in the accretion rates once isolated ponds connect to the channel network. This model is used to generate the simulations shown in Figure 5A.

We assume that, above a critical elevation Z_c for marsh recovery (see "Model approach" in the main text), marshes are widespread and both inorganic and organic accretion contributes to $\partial_t Z$. In that case, $\partial_t Z = A_i(x,Z,t)+A_o(D)-R$, where $A_o(D)$ is the depth-dependent organic accretion rate (by definition $D=\delta z/2-Z$). We assume that, for elevations below Z_c but above an arbitrary lower elevation Z_t, marshes drown ($A_o=0$) and form isolated ponds with no net inorganic accretion ($A_i=0$). Thus, the average deepening rate of an isolated pond equals the rate of RSLR: $\partial_t Z = -R$. Finally, when the pond elevation is below Z_t, we assume ponds connect to the channel network and reach an equilibrium depth slightly lower than Z_t, and thus $\partial_t Z = 0$.

The minimal marsh model has the form:

$$\partial_t Z = \begin{cases} A_i(x,Z,t)+A_o(D)-R & \text{for } Z>Z_c \\ -R & \text{for } Z_t<Z\le Z_c. \\ 0 & \text{for } Z\le Z_t \end{cases} \qquad \text{(Equation 15)}$$

Since we are primarily interested in drowning marshes, for which $R>\max\{A_o\}$ and thus are closer to the critical elevation Z_c, we assume for simplicity a constant accretion rate A_o in the range $A_o^c\le A_o\le\max\{A_o\}$, where $A_o^c = A_o(D_c)$ is the organic accretion rate at the critical depth ($D_c = \delta z/2 - Z_c$).

The inorganic accretion rate $A_i(x,Z,t)$ is given by Equation 14 and can be written in terms of the critical accretion rate in the marsh interior, $A_i^c(L) = A_i(L,D_c)$, as:

$$A_i(x,Z,t) = A_i^c(L)\frac{\tau(Z)}{\tau(Z_c)}\exp\left(\frac{1-\ell(x,t)}{\ell_c}\right), \qquad \text{(Equation 16)}$$

where $\tau(Z) = \pi^{-1}\arccos(2Z/\delta z)$ is the rescaled inundation time at elevation Z, $\ell_c = \beta/w_f^+$ is the rescaled decay length $\ell_c = L_c/L$, and the function $\ell(x,t) \in [0,1]$ is defined as the distance from the edge of a channel (or connected pond) rescaled such that $\ell = 1$ at the corresponding watershed divide (e.g., $\ell(x) = x/L$ if the marsh edge is at $x = 0$ and the watershed divide at $x = L$).

A further simplification is obtained by approximating $\pi^{-1}\arccos(x)$ by $(1-x)/2$ in the rescaled inundation time τ, which gives

$$\tau(Z) = \frac{1}{2} - \frac{Z(x,t)}{\delta z}. \qquad \text{(Equation 17)}$$

Using $Z_c/\delta z = 0.15$ as the critical elevation for marshes (corresponding to $D_c = 0.35\delta z$, see Figure 1) we get $\tau(Z_c) = 0.35$.

The function $\ell(x,t)$ in Equation 16 generalizes the concept of the distance x to the marsh edge to account for the formation of new connected ponds. We assume that connected ponds change the geometry of the drainage basin and become a new source of both tidal water and inorganic sediment with concentration C_0. As ponds get deeper than Z_t and connect to the channel network, we update the term $\ell(x,t)$ to reflect the positions x_j of the new marsh edges (defined by the condition $Z(x_j) = Z_t$), and corresponding watershed divides (defined as the midpoint between neighboring channels or connected ponds.)

For the numerical integration of Equations 15, 16, and 17, rates are rescaled by the drowning threshold $R_c = A_o + A_i^c(L)$, lengths are rescaled by the initial domain size L_0, elevations are rescaled by tidal range δz, and times are rescaled by $\delta z/R_c$. Since $A_i^c(L) = R_c - A_o$, by definition the model has five dimensionless parameters: R/R_c, A_o/R_c, ℓ_c, $Z_c/\delta z$, and $Z_t/\delta z$.

For the simulations shown in Figure 5A, we choose values representative of a microtidal marsh with moderate sediment supply: $\delta z = 1$ m and $C_0 = 50$ g/m^3, with $A_o = 3$ mm/year, $w_f = 10^{-4}$ m/s, and $T = 12.5$ h. We thus get $A_o/R_c = 0.78$ and $\ell_c = 1/3$. We use a rescaled critical elevation $Z_c/\delta z = 0.15$, consistent with field data (Figure 1B), and assume ponds with a depth around MSL connect to channels, thus $Z_t/\delta z = 0$. We change the rescaled RSLR rates R/R_c in the range 0.8–5. The initial condition is a marsh platform of rescaled elevation $Z/\delta z = 0.4$ and unit rescaled length, limited by tidal channels at both sides. For the pond size distributions shown in Figure 5B, we choose a 10 km domain size.

Scaling of the equilibrium pond size L_p

The scale invariance of spatial sediment deposition patterns leads to a similar scale invariance in the size, or diameter L_p, of the resulting ponds. Assuming the edge of the pond, a distance $x_p = L - L_p/2$ from the channel bank, is at equilibrium with RSLR at the critical depth D_c, then $R = A_o^c + A_i^c(x_p)$ (Equation 15). Substituting Equation 16 with $Z(x_p) = Z_c$ and rescaled position of the pond edge $\ell(x_p) = x_p/L = 1 - L_p/(2L)$, and using the definition of the drowning threshold $R_c = A_o^c + A_i^c(L)$, the rescaled equilibrium pond size is

$$\frac{L_p}{L} = 2\ell_c \ln\left(\frac{R - A_o^c}{R_c - A_o^c}\right), \qquad \text{(Equation 18)}$$

where, $\ell_c = \beta/w_f^+ = \beta\delta z/(Tw_f)$ is the rescaled sediment concentration decay length.

The rescaled equilibrium pond size (Equation 18) has two limits: no permanent ponds ($L_p = 0$) for $R \le R_c$, and no marshes ($L_p = 2L$) above the highest drowning threshold at marsh edge, $R \ge A_o^c + A_i^c(0) = A_o^c + (R_c - A_o^c)\exp(1/\ell_c)$ (Figure 5A). Note that this pond size is a minimum value as we assume no lateral pond erosion besides marsh drowning.

Analysis and interpretation of inorganic accretion data

To only test the dependence on the distance to channel, reported accretion rates A_i for Phillips Creek (Figure 3D) were depth-corrected to eliminate the scaling with the flooding frequency: $A_i^* = A_i\tau(\overline{D})/\tau(D)$, where $\tau(D) = \pi^{-1}\arccos(1-2D/\delta z)$ is the approximated rescaled inundation time and $\overline{D}$ is the mean marsh depth. We could not perform a similar correction for Norfolk (Figure 3E) because of lack of detailed elevation data. However, the fact this marsh is relatively young and has not reached a steady-state elevation yet suggests that the noticeable exponential decay in both the 5-year average accretion rates and the values during individual tides is mainly due to the spatial gradient of sediment distribution.[21] For the Bay of Fundy, there is no obvious trend in accretion rates as they were poorly correlated with both marsh elevation (for the relevant range above 5.2 m) and distance to channel (Figure 3F). However, this is consistent with our prediction for very large tidal ranges (Equation 2).

SUPPLEMENTAL INFORMATION

Supplemental information can be found online at https://doi.org/10.1016/j.oneear.2021.02.013.

ACKNOWLEDGMENTS

We acknowledge Lennert Schepers for kindly providing some of the pond area data. This work was funded by the National Science Foundation Coastal SEES (no. 1426981), GLD (no. 1529245), CAREER (no. 1654374), and LTER (no. 1237733) programs. O.D.V. acknowledges the support of the Texas A&M Engineering Experiment Station (TEES).

AUTHOR CONTRIBUTIONS

Conceptualization, O.D.V., E.R.H., and M.L.K.; methodology, O.D.V.; software, O.D.V.; investigation, O.D.V.; writing – original draft, O.D.V., E.R.H., and M.L.K.; writing – review & editing, O.D.V., E.R.H., and M.L.K.; validation, O.D.V., D.J.C., and J.D.H.; funding acquisition, M.L.K.

DECLARATION OF INTERESTS

The authors declare no competing interests.

Received: September 17, 2019
Revised: January 23, 2021
Accepted: February 23, 2021
Published: March 25, 2021

REFERENCES

1. Morris, J.T., Barber, D.C., Callaway, J.C., Chambers, R., Hagen, S.C., Hopkinson, C.S., Johnson, B.J., Megonigal, P., Neubauer, S.C., Troxler, T., and Wigand, C. (2016). Contributions of organic and inorganic matter to sediment volume and accretion in tidal wetlands at steady state: sediment bulk density and ignition loss. Earth's Future *4*, 110–121, https://doi.org/10.1002/2015EF000334.
2. Kirwan, M.L., Temmerman, S., Skeehan, E.E., Guntenspergen, G.R., and Fagherazzi, S. (2016). Overestimation of marsh vulnerability to sea level rise. Nat. Clim. Change *6*, 253–260, https://doi.org/10.1038/nclimate2909.
3. Marani, M., D'Alpaos, A., Lanzoni, S., Carniello, L., and Rinaldo, A. (2007). Biologically-controlled multiple equilibria of tidal landforms and the fate of the Venice Lagoon. Geophys. Res. Lett. *34*, https://doi.org/10.1029/2007GL030178.
4. Fagherazzi, S., Kirwan, M.L., Mudd, S.M., Guntenspergen, G.R., Temmerman, S., Rybczyk, J.M., Reyes, E., Craft, C., and Clough, J. (2012). Numerical models of salt marsh evolution: ecological, geomorphic, and climatic factors. Rev. Geophys. 1–28, https://doi.org/10.1029/2011RG000359.
5. Kolker, A.S., Kirwan, M.L., Goodbred, S.L., and Cochran, J.K. (2010). Global climate changes recorded in coastal wetland sediments: empirical observations linked to theoretical predictions. Geophys. Res. Lett. *37*, https://doi.org/10.1029/2010GL043874.

6. Hill, T.D., and Anisfeld, S.C. (2015). Coastal wetland response to sea level rise in Connecticut and New York. Estuar. Coast. Shelf Sci. *163*, 185–193, https://doi.org/10.1016/j.ecss.2015.06.004.

7. Alizad, K., Hagen, S.C., Morris, J.T., Medeiros, S.C., Bilskie, M.V., and Weishampel, J.F. (2016). Coastal wetland response to sea-level rise in a fluvial estuarine system. Earth's Future *4*, 483–497, https://doi.org/10.1002/2016EF000385.

8. Alizad, K., Hagen, S.C., Medeiros, S.C., Bilskie, M.V., Morris, J.T., Balthis, L., and Buckel, C.A. (2018). Dynamic responses and implications to coastal wetlands and the surrounding regions under sea level rise. PLoS One *13*, e0205176, https://doi.org/10.1371/journal.pone.0205176.

9. Day, J., Ibáñez, C., Scarton, F., Pont, D., Hensel, P., Day, J., and Lane, R. (2011). Sustainability of Mediterranean deltaic and lagoon wetlands with sea-level rise: the importance of river input. Estuaries Coast. *34*, 483–493, https://doi.org/10.1007/s12237-011-9390-x.

10. Kirwan, M.L., and Megonigal, J.P. (2013). Tidal wetland stability in the face of human impacts and sea-level rise. Nature *504*, 53–60, https://doi.org/10.1038/nature12856.

11. Kearney, M.S. (2016). Microtidal marshes: can these widespread and fragile marshes survive increasing climate-sea level variability and human action? J. Coast. Res. *32*, 686, https://doi.org/10.2112/JCOASTRES-D-15-00069.1.

12. D'Alpaos, A., Mudd, S.M., and Carniello, L. (2011). Dynamic response of marshes to perturbations in suspended sediment concentrations and rates of relative sea level rise. J. Geophys. Res. Earth Surf. *116*, https://doi.org/10.1029/2011JF002093.

13. Kirwan, M.L., Guntenspergen, G.R., D'Alpaos, A., Morris, J.T., Mudd, S.M., and Temmerman, S. (2010). Limits on the adaptability of coastal marshes to rising sea level. Geophys. Res. Lett. *37*, https://doi.org/10.1029/2010GL045489.

14. Turner, R.E., Swenson, E.M., and Milan, C.S. (2002). Organic and inorganic contributions to vertical accretion in salt marsh sediments. In Concepts and Controversies in Tidal Marsh Ecology (Springer), pp. 583–595, https://doi.org/10.1007/0-306-47534-027.

15. Nyman, J.A., Walters, R.J., Delaune, R.D., and Patrick, W.H. (2006). Marsh vertical accretion via vegetative growth. Estuar. Coast. Shelf Sci. *69*, 370–380, https://doi.org/10.1016/j.ecss.2006.05.041.

16. Neubauer, S.C. (2008). Contributions of mineral and organic components to tidal freshwater marsh accretion. Estuar. Coast. Shelf Sci. *78*, 78–88, https://doi.org/10.1016/j.ecss.2007.11.011.

17. Kirwan, M.L., and Guntenspergen, G.R. (2012). Feedbacks between inundation, root production, and shoot growth in a rapidly submerging brackish marsh. J. Ecol. *100*, 764–770, https://doi.org/10.1111/j.1365-2745.2012.01957.x.

18. D'Alpaos, A. (2011). The mutual influence of biotic and abiotic components on the long-term ecomorphodynamic evolution of salt-marsh ecosystems. Geomorphology *126*, 269–278, https://doi.org/10.1016/j.geomorph.2010.04.027.

19. Ratliff, K.M., Braswell, A.E., and Marani, M. (2015). Spatial response of coastal marshes to increased atmospheric CO_2. Proc. Natl. Acad. Sci. U S A. 201516286. https://doi.org/10.1073/pnas.1516286112.

20. D'Alpaos, A., and Marani, M. (2016). Reading the signatures of biologic-geomorphic feedbacks in salt-marsh landscapes. Adv. Water Resour. *93, Part B*, 265–275, https://doi.org/10.1016/j.advwatres.2015.09.004.

21. French, J.R., and Spencer, T. (1993). Dynamics of sedimentation in a tide-dominated backbarrier salt marsh, Norfolk, UK. Mar. Geol. *110*, 315–331.

22. Christiansen, T., Wiberg, P., and Milligan, T. (2000). Flow and sediment transport on a tidal salt marsh surface. Estuar. Coast. Shelf Sci. *50*, 315–331, https://doi.org/10.1006/ecss.2000.0548.

23. Temmerman, S., Govers, G., Wartel, S., and Meire, P. (2003). Spatial and temporal factors controlling short-term sedimentation in a salt and freshwater tidal marsh, Scheldt estuary, Belgium, SW Netherlands. Earth Surf. Process. Landf. *28*, 739–755.

24. Reed, D.J. (1995). The response of coastal marshes to sea-level rise: survival or submergence? Earth Surf. Process. Landf. *20*, 39–48, https://doi.org/10.1002/esp.3290200105.

25. Fagherazzi, S., Wiberg, P.L., Temmerman, S., Struyf, E., Zhao, Y., and Raymond, P.A. (2013). Fluxes of water, sediments, and biogeochemical compounds in salt marshes. Ecol. Process. *2*, 3, https://doi.org/10.1186/2192-1709-2-3.

26. Temmerman, S., Bouma, T.J., Govers, G., Wang, Z.B., De Vries, M.B., and Herman, P.M.J. (2005). Impact of vegetation on flow routing and sedimentation patterns: three-dimensional modeling for a tidal marsh. J. Geophys. Res. Earth Surf. *110*, https://doi.org/10.1029/2005JF000301.

27. D'Alpaos, A., Lanzoni, S., Marani, M., and Rinaldo, A. (2007). Landscape evolution in tidal embayments: modeling the interplay of erosion, sedimentation, and vegetation dynamics. J. Geophys. Res. Earth Surf. *112*, F01008, https://doi.org/10.1029/2006JF000537.

28. Da Lio, C., D'Alpaos, A., and Marani, M. (2013). The secret gardener: vegetation and the emergence of biogeomorphic patterns in tidal environments. Philos. Trans. R. Soc. A Math. Phys. Eng. Sci. *371*, 20120367, https://doi.org/10.1098/rsta.2012.0367.

29. Belliard, J.P., Di Marco, N., Carniello, L., and Toffolon, M. (2016). Sediment and vegetation spatial dynamics facing sea-level rise in microtidal salt marshes: insights from an ecogeomorphic model. Adv. Water Resour. *93*, 249–264, https://doi.org/10.1016/j.advwatres.2015.11.020.

30. Mudd, S.M., D'Alpaos, A., and Morris, J.T. (2010). How does vegetation affect sedimentation on tidal marshes? Investigating particle capture and hydrodynamic controls on biologically mediated sedimentation. J. Geophys. Res. *115*, https://doi.org/10.1029/2009JF001566.

31. Roner, M., D'Alpaos, A., Ghinassi, M., Marani, M., Silvestri, S., Franceschinis, E., and Realdon, N. (2016). Spatial variation of salt-marsh organic and inorganic deposition and organic carbon accumulation: inferences from the Venice Lagoon, Italy. Adv. Water Resour. *93, Part B*, 276–287, https://doi.org/10.1016/j.advwatres.2015.11.011.

32. Ganju, N.K., Kirwan, M.L., Dickhudt, P.J., Guntenspergen, G.R., Cahoon, D.R., and Kroeger, K.D. (2015). Sediment transport-based metrics of wetland stability: sediment metrics of wetland stability. Geophys. Res. Lett. *42*, 7992–8000, https://doi.org/10.1002/2015GL065980.

33. Ganju, N.K., Defne, Z., Kirwan, M.L., Fagherazzi, S., D'Alpaos, A., and Carniello, L. (2017). Spatially integrative metrics reveal hidden vulnerability of microtidal salt marshes. Nat. Commun. *8*, https://doi.org/10.1038/ncomms14156.

34. Christiansen, T. (1998). Sediment Deposition on a Tidal Salt Marsh, Ph.D. thesis (Charlottesville: University of Virginia).

35. Coleman, D.J., and Kirwan, M.L. (2019). The effect of a small vegetation dieback event on salt marsh sediment transport. Earth Surf. Process. Landf. *44*, 944–952, https://doi.org/10.1002/esp.4547.

36. Morris, J.T., Sundareshwar, P.V., Nietch, C.T., Kjerfve, B., and Cahoon, D.R. (2002). Responses of coastal wetlands to rising sea level. Ecology *83*, 2869–2877.

37. French, J. (2006). Tidal marsh sedimentation and resilience to environmental change: exploratory modelling of tidal, sea-level and sediment supply forcing in predominantly allochthonous systems. Mar. Geol. *235*, 119–136, https://doi.org/10.1016/j.margeo.2006.10.009.

38. Carniello, L., Defina, A., and D'Alpaos, L. (2012). Modeling sand-mud transport induced by tidal currents and wind waves in shallow microtidal basins: application to the Venice Lagoon (Italy). Estuar. Coast. Shelf Sci. *102-103*, 105–115, https://doi.org/10.1016/j.ecss.2012.03.016.

39. Marani, M., Lio, C.D., and D'Alpaos, A. (2013). Vegetation engineers marsh morphology through multiple competing stable states. Proc. Natl. Acad. Sci. U S A *110*, 3259–3263, https://doi.org/10.1073/pnas.1218327110.

40. Mariotti, G. (2016). Revisiting salt marsh resilience to sea level rise: are ponds responsible for permanent land loss? J. Geophys. Res. Earth Surf. *121*, 1391–1407, https://doi.org/10.1002/2016JF003900.

41. Schepers, L., Kirwan, M., Guntenspergen, G., and Temmerman, S. (2017). Spatio-temporal development of vegetation die-off in a submerging

coastal marsh: spatio-temporal marsh die-off. Limnol. Oceanogr. *62*, 137–150, https://doi.org/10.1002/lno.10381.

42. Wilson, C.A., Hughes, Z.J., FitzGerald, D.M., Hopkinson, C.S., Valentine, V., and Kolker, A.S. (2014). Saltmarsh pool and tidal creek morphodynamics: dynamic equilibrium of northern latitude saltmarshes? Geomorphology *213*, 99–115, https://doi.org/10.1016/j.geomorph.2014.01.002.
43. van Belzen, J., van de Koppel, J., Kirwan, M.L., van der Wal, D., Herman, P.M.J., Dakos, V., Kéfi, S., Scheffer, M., Guntenspergen, G.R., and Bouma, T.J. (2017). Vegetation recovery in tidal marshes reveals critical slowing down under increased inundation. Nat. Commun. *8*, 15811, https://doi.org/10.1038/ncomms15811.
44. Rinaldo, A., Fagherazzi, S., Lanzoni, S., Marani, M., and Dietrich, W.E. (1999). Tidal networks 2. Watershed delineation and comparative network morphology. Water Resour. Res. *35*, 3905–3917.
45. Belliard, J.-P., Toffolon, M., Carniello, L., and D'Alpaos, A. (2015). An ecogeomorphic model of tidal channel initiation and elaboration in progressive marsh accretional contexts. J. Geophys. Res. Earth Surf. *120*, 1040–1064, https://doi.org/10.1002/2015JF003445.
46. Wang, C., and Temmerman, S. (2013). Does biogeomorphic feedback lead to abrupt shifts between alternative landscape states? An empirical study on intertidal flats and marshes. J. Geophys. Res. Earth Surf. *118*, 229–240, https://doi.org/10.1029/2012JF002474.
47. Defina, a., Carniello, L., Fagherazzi, S., and D'Alpaos, L. (2007). Self-organization of shallow basins in tidal flats and salt marshes. J. Geophys. Res. *112*, F03001, https://doi.org/10.1029/2006JF000550.
48. Fagherazzi, S., Carniello, L., D'Alpaos, L., and Defina, A. (2006). Critical bifurcation of shallow microtidal landforms in tidal flats and salt marshes. Proc. Natl. Acad. Sci. U S A *103*, 8337–8341, https://doi.org/10.1073/pnas.0508379103.
49. Wang, C., Schepers, L., Kirwan, M.L., Belluco, E., D'Alpaos, A., Wang, Q., Yin, S., and Temmerman, S. (2021). Different coastal marsh sites reflect similar topographic conditions under which bare patches and vegetation recovery occur. Earth Surf. Dyn. *9*, 71–88, https://doi.org/10.5194/esurf-9-71-2021.
50. Claudin, P., Charru, F., and Andreotti, B. (2011). Transport relaxation time and length scales in turbulent suspensions. J. Fluid Mech. *671*, 491–506, https://doi.org/10.1017/S0022112010005823.
51. Coleman, D.J., Ganju, N.K., and Kirwan, M.L. (2020). Sediment delivery to a tidal marsh platform is minimized by source decoupling and flux convergence. J. Geophys. Res. Earth Surf. https://doi.org/10.1029/2020JF005558.
52. van Proosdij, D., Davidson-Arnott, R.G., and Ollerhead, J. (2006). Controls on spatial patterns of sediment deposition across a macro-tidal salt marsh surface over single tidal cycles. Estuar. Coast. Shelf Sci. *69*, 64–86, https://doi.org/10.1016/j.ecss.2006.04.022.
53. Temmerman, S., Govers, G., Wartel, S., and Meire, P. (2004). Modelling estuarine variations in tidal marsh sedimentation: response to changing sea level and suspended sediment concentrations. Mar. Geol. *212*, 1–19, https://doi.org/10.1016/j.margeo.2004.10.021.
54. Himmelstein, J.D. (2018). Mechanisms of Pond Expansion on the Saltmarshes of the Blackwater National Wildlife Refuge, Master's thesis (The College of William and Mary).
55. Ortiz, A.C., Roy, S., and Edmonds, D.A. (2017). Land loss by pond expansion on the Mississippi River Delta Plain. Geophys. Res. Lett. *44*, 3635–3642, https://doi.org/10.1002/2017GL073079.
56. Mariotti, G., Kearney, W., and Fagherazzi, S. (2016). Soil creep in salt marshes. Geology. G37708.1. https://doi.org/10.1130/G37708.1.
57. Newman, M. (2005). Power laws, Pareto distributions and Zipf's law. Contemp. Phys. *46*, 323–351, https://doi.org/10.1080/00107510500052444.
58. Stevenson, J.C., Kearney, M.S., and Pendleton, E.C. (1985). Sedimentation and erosion in a Chesapeake Bay brackish marsh system. Mar. Geol. *67*, 213–235.
59. Törnqvist, T.E., Jankowski, K.L., Li, Y.-X., and González, J.L. (2020). Tipping points of Mississippi Delta marshes due to accelerated sea-level rise. Sci. Adv. *6*, eaaz5512, https://doi.org/10.1126/sciadv.aaz5512.
60. Reef, R., Spencer, T., Möller, I., Lovelock, C.E., Christie, E.K., McIvor, A.L., Evans, B.R., and Tempest, J.A. (2017). The effects of elevated CO_2 and eutrophication on surface elevation gain in a European salt marsh. *Glob. Change Biol.* *23*, 881–890, https://doi.org/10.1111/gcb.13396.
61. DeLaune, R.D., Whitcomb, J.H., Patrick, W.H., Pardue, J.H., and Pezeshki, S.R. (1989). Accretion and canal impacts in a rapidly subsiding wetland. I. 137 Cs and 210 Pb techniques. Estuaries Coast. *12*, 247–259.
62. Burdick, D.M., Moore, G.E., Adamowicz, S.C., Wilson, G.M., and Peter, C.R. (2019). Mitigating the legacy effects of ditching in a New England salt marsh. Estuaries Coast. https://doi.org/10.1007/s12237-019-00656-5.
63. Mariotti, G., and Fagherazzi, S. (2013). Critical width of tidal flats triggers marsh collapse in the absence of sea-level rise. Proc. Natl. Acad. Sci. U S A *110*, 5353–5356, https://doi.org/10.1073/pnas.1219600110.
64. Schuerch, M., Spencer, T., Temmerman, S., Kirwan, M.L., Wolff, C., Lincke, D., McOwen, C.J., Pickering, M.D., Reef, R., Vafeidis, A.T., et al. (2018). Future response of global coastal wetlands to sea-level rise. Nature *561*, 231–234, https://doi.org/10.1038/s41586-018-0476-5.